Optics & Laser Technology 168 (2024) 109963

Contents lists available at ScienceDirect

Optics and Laser Technology

journal homepage: www.elsevier.com/locate/optlastec

Full length article

Predictive models based on RSM and ANN for roughness and wettability achieved by laser texturing of S275 carbon steel alloy

F. Bañon [a,*], S. Martin [a], J.M. Vazquez-Martinez [b], J. Salguero [c], F.J. Trujillo [a]

[a] Department of Civil, Materials and Manufacturing Engineering, University of Malaga, Malaga, Spain
[b] Department of Civil and Industrial Engineering, Algeciras Higher Technical School of Engineering, University of Cadiz, Av. Ramon Puyol s/n, E11202 Algeciras, Spain
[c] Department of Mechanical Engineering and Industrial Design, School of Engineering, University of Cadiz, Spain

ARTICLE INFO

Keywords:
Roughness
Wettability
ANN
RSM
Steel
LST

ABSTRACT

Laser texturing is increasingly gaining attention in the field of metal alloys due to its ability to improve surface properties, particularly in steel alloys. However, the input parameters of the technology must be carefully controlled to achieve the desired surface roughness. Roughness is critical to the activation of the surface before further bonding operations, and it is often assessed using several parameters such as *Ra*, *Rt*, *Rz*, and *Rv*. This surface activation affects the properties of the metal alloy in terms of wettability, which has been evaluated by the deposition of ethylene glycol droplets through a contact angle. This allowed a direct relationship to be established between the final roughness, the wettability of the surface and the texturing parameters of the alloy.

This raises the interest of being able to predict the behaviour in terms of roughness and wettability for future applications in improving the behaviour of metallic alloys. In this research, a comparative analysis between Response Surface Models (*RSM*) and predictive models based on Artificial Neural Networks (*ANN*) has been conducted. The model based on neural networks was able to predict all the output variables with a fit greater than 90%., improving that obtained by *RSM*. The model obtained by ANN allows a greater adaptability to the variation of results obtained, reaching deviations close to 0.2 μm. The influence of input parameters, in particular power and scanning speed, on the achieved roughness and surface wettability has been figured out by contact angle measurements. This increases its surface activation in terms of wettability. Superhydrophilic surfaces were achieved by setting the power to 20 W and scanning speed to ten mm/s. In contrast, a power of 5 W and a scanning speed of 100 mm/s reduced the roughness values.

1. Introduction

Laser Surface Texturing (LST) is a technique that has gained interest recently due to its numerous applications in improving the surface properties of materials [1]. This technique is based on the generation of micro and nanostructures on the surface of the material using a high - energy laser beam [2].

Current lines of research in laser texturing of metal alloys are focused on controlling the roughness obtained by generating micro-geometrical patterns or textures [3]. This can be achieved using new laser processing techniques that allow greater control over texture formation [4,5]. In addition, new metal alloys are being developed, which can be textured by LST to improve their surface properties[6]. Some authors [7], indicate that surface pre-treatment and laser texturing can improve the strength of joints between aluminium alloys and polymers in friction lap welding.

Another research area is the integration of LST with other material processing techniques, such as thin film deposition or heat treatment. The results obtained in [8] conclude that the hardness of 5A06 aluminium alloy can be improved through LST, with scanning speed being the most significant parameter [9]. Combining these techniques can further improve the surface properties of materials and enable the creation of surfaces with multifunctional characteristics [7].

The main parameters of laser texturing are laser wavelength, Power, pulse repetition frequency, scanning speed, and beam spot size [10]. Thus, laser energy is one of the most critical parameters in laser texturing as it directly affects the quality of the created surface [11]. If the energy is too low, the microstructures may not be well defined, and the surface quality may be poor. If the energy is too high, the microstructures may melt, and the surface may show irregularities and excessive porosity. In [12], the authors found that well defined textured

* Corresponding author.
E-mail address: fermin.banon@uma.es (F. Bañon).

https://doi.org/10.1016/j.optlastec.2023.109963
Received 18 May 2023; Received in revised form 24 July 2023; Accepted 18 August 2023
Available online 22 August 2023

surfaces are obtained with low laser power (1% of the maximum working power of 30 W) and medium scanning speeds (500 mm/s). On the other hand, too high -speed, upper than 500 mm/s, can result in a surface with excessive irregularities and roughness, while too low speed, close to 100 mm/s, can result in a surface with less defined microstructures and poor surface quality.

The choice of these parameters depends on the properties of the material to be processed and the type of surface texture desired [13]. For example, a higher beam intensity can generate a deeper texture on the surface of the material, while a lower scanning speed can generate a finer and more uniform texture [14]. However, according to the roughness results, the laser texturing frequency parameter has less effect on surface texture compared to other parameters such as average power and scanning speed [15].

Surface activation is a process by which the surface properties of a material are modified or enhanced to promote specific interactions or reactions with other substances. The purpose of surface activation is to increase the surface energy or reactivity of a material, thereby improving its adhesion, wetting or bonding properties [8]. In general, an increase in the roughness after laser surface texturing can improve the surface activation of the surface as they all supply a larger contact area for adhesion [16]. However, an excessive increase in roughness can have negative effects on surface strength and durability. Therefore, it is important to find a balance between roughness and mechanical strength to obtain best surface activation [17].

Roughness is one of the key factors in laser texturing as it is related to surface activation [17]. A rough surface increases the contact area between the material and other elements, which improves the bonding ability and adhesion of coatings and paints [18]. On the other hand, hydrophilic surfaces have a high affinity for water, while hydrophobic surfaces have a low affinity [19]. Laser texturing is used to create hydrophobic surfaces by creating micro textures that prevent water from adhering to the surface. In the research developed in [20], the authors discuss the use of LST for creating super-hydrophobic surfaces and their potential applications.

The influence of the laser texturing parameters on the roughness parameters *Ra*, *Rt*, *Rz*, and *Rv* is highly significative for the quality of the resulting surface [21,22]. The *Ra* value refers to the average roughness of the surface. The *Rt* value refers to the maximum height of the irregularity on the evaluated profile, while the *Rz* value refers to the height of the irregularities in each of the evaluation length of the measured profile. Finally, the *Rv* value refers to the depth of the rough surface. In general, increasing the beam intensity and decreasing the scanning speed, the surface roughness values can be reduced [23,24]. However, these roughness values can vary depending on the type of metal alloy to be processed.

S275 carbon steel is a type of structural steel used in a wide variety of applications, from construction to machine and tool making. Laser texturing has proven to be an effective technique for improving the adhesion and corrosion resistance of this type of steel, which can improve its durability and its ability to withstand loads and stresses. Laser texturing can generate micro texture patterns that improve the adhesion of paints and coatings on the surface of S275 carbon steel, which in turn improves its corrosion resistance [25]. In this way, laser texturing has proven to be effective in increasing corrosion resistance in aggressive environments, such as in the maritime or petrochemical industry [26–28]. It has been shown that laser texturing can increase the hydrophobicity of the steel surface, making it suitable for applications where high corrosion resistance is needed [28,29].

Although LST has been successfully applied on various materials, there are some limitations in its application on metallic alloys. Due to the thermal processing of the laser beam, porosity formation and cracking are common problems in laser texturing of metallic alloys, which limit the quality of texture and lifetime of the material. It can also present limitations in terms of the shape and depth of texture that can be generated [29]. For example, the texture may be limited to certain geometric patterns, and the depth of the texture may be limited by the laser energy and scanning speed.

The use of predictive models reduces the number of experimental tests and material costs. This is of great benefit to the industry as it allows predicting micro and macro geometric defects based on input parameter values and finding areas of sufficient quality without additional testing. In laser texturing, Response Surface Methodology (*RSM*) is used as a model to predict the results of the process. This statistical approach involves creating a mathematical model that relates the input parameters (laser texturing parameters) to the output variables (such as roughness, hydrophobicity, and surface activation) [30].

Using *RSM*, the best results in terms of roughness and surface activation can be achieved by optimising the input parameters. Although *RSM* is a useful tool for predicting laser texturing results, its accuracy is limited for complex and nonlinear processes. It depends on the quality of the experimental data used to train the model [31,32].

Usually, machining regression models are focused on the prediction of a single output variable, and there are few models capable of involving several output variables simultaneously, given the complexity of the machining processes [33]. Nevertheless, the great evolution that computational techniques have undergone recently makes it possible to develop automatic learning algorithms capable of autonomously adjusting the machining parameters to achieve a specific objective [36]. The use of these algorithms is part of what is called “intelligent machining”, which includes the development of interactions with different systems (machine tools, sensors, controllers, simulation-based designs, big data, and cloud computing systems) [34]. In this regard, Artificial Neural Networks (*ANN*) are one of the most used algorithms to model machining operations [35,36].

Neural networks are a potentially more correct, flexible, and faster alternative to response surface methodologies for predicting laser texturing results. The learning capability of neural networks and their flexibility to manage nonlinear and non-Gaussian data make them ideal for modelling complex, nonlinear processes [37].

The outcome prediction using an application of neural networks offers advantages over response surface methodology in laser texturing [38,39]. Neural networks are capable of handling substantial amounts of data, which allow for greater accuracy in predicting results. In addition, neural networks can detect complex patterns and relationships in data that are not detectable using *RSM* [40]. Neural networks can learn from large data sets and discover patterns not clear in the input data. In comparison, *RSM* techniques often require a mathematical function that can be fitted to the experimental data, which can limit their ability to discover complex patterns.

Among metal alloys, laser texturing of steels has generated a steady scientific production with increasing trend in the last ten years [41,42]. There is also a recent interest in the prediction of results in the last ten years, mainly based on *RSM* techniques and more recently through the application of *ANN* techniques.

This study aimed to evaluate the relationship between surface roughness and wettability in laser-textured patterns of S275 carbon steel. The study shows that energy density, scanning speed, and frequency significantly affect surface roughness, which in turn affects wettability. The input parameters considered were power, frequency, and scanning speed, while the output parameters were Ra, Rt, Rz, and Rv for roughness and contact angle in wetting tests. The control of the obtained roughness and the relationship between the input parameters and surface activation, in terms of wettability, is essential to improve the quality of materials in hybrid structures, such as S275, used for joining dissimilar materials [43,44]. These structures combine the structural properties of carbon steel with the mechanical performance/density ratio of composite materials. This makes them strategic materials for the automotive and construction sectors [45,46]. The proper control of surface roughness and activation through laser texturing techniques can improve the quality of material bonding [47,48].

The roughness generated on metallic surfaces after texturing

Table 1
S275 carbon steel alloy composition and principal mechanical properties.

Fe	%Mn	%C	Si	%S	%P
98.01	1.60	0.25	0.05	0.05	0.04

Yield Strength (MPa)	Tensile Strength (MPa)
275	450

Table 2
Levels set for input parameters in laser texturing.

Power-P (W)	Frequency-F (kHz)	Scanning speed-SS (mm/s)
5–10–20	20–80	10–100–250

treatments is a key area for subsequent operations [49]. In this research, a complete characterisation of the generated roughness and its wettability was obtained for different combinations of laser texturing. The influence of the input parameters on the generated roughness and the relationship between the generated roughness, the wettability in terms of contact angle and the energy density of the laser beam for different scanning speeds has been established.

Furthermore, in this research, the comparison between two methods for predicting results has been deepened by establishing a comparison between models widely used in nonconventional technologies based on the response surface and a prediction based on neural networks. The aim is to obtain a methodology capable of predicting all the studied parameters that characterise the behaviour of the surface obtained after a texturing operation, thus achieving the best possible adaptation.

Predictive models using response surface and neural networks have been developed to predict surface roughness and wettability as a function of texturing parameters. Response surface methodology (*RSM*) is particularly suitable for unconventional machining processes due to the variety of input parameters. However, neural network models have been used to supply higher accuracy and better fit for a broad range of output variables compared to response surface models, which can only predict a single output variable. This has been confirmed by the results of this study, as well as a correlation between roughness and surface activation after laser texturing tests.

2. Methodology

Specimens of S275 carbon steel with an area of 10x10 mm^2 and thickness of 3 mm were used to evaluate the influence of laser texturing treatments. Mechanical properties and composition (% mass) of steel specimens are shown in Table 1.

The experimental design consisted of a combination of different levels of power, frequency, and scanning speed, as shown in Table 2. A Rofin Easymark F20 Ytterbium laser equipment was used in the texturing study (Fig. 1.a).

All tests were performed with a wavelength of 1062 nm and focal length of 185 mm, resulting in a spot diameter of 60 µm and a distance between lines of 50 µm. The texturing area was 10x10 mm^2, and all samples were generated supporting a bidirectional shading distribution with a laser beam overlapping in a pattern of straight parallel lines (Fig. 2).

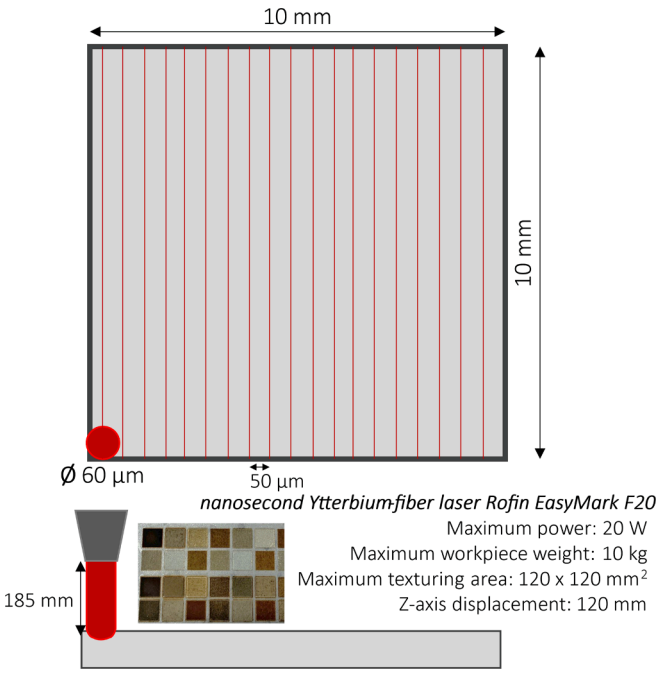

Fig. 2. Texturing pattern established in the experimental design and main characteristics of the laser equipment.

After the texturing trials, surface quality was evaluated in terms of Average Roughness (*Ra)*, Maximum peak to valley height (*Rt)*, Mean roughness depth (*Rz)*, and maximum profile valley depth (*Rv)*. The equipment used was a Mahr Perthometer PGK 120 roughness measurement station (Fig. 1.b). ISO 4287 standard was followed, and three measurements were taken perpendicular to the texturing pattern.

The aim of this work is to achieve surface activation of the steel alloy by laser texturing. Surface activation refers to the ability to modify the properties of the metallic alloy and improve its adhesion or liquid absorption capacity.

This surface activation is directly related to the roughness created on the surface and its wettability (Fig. 3.a). The surface roughness of the substrate must be capable of allowing the adhesive to flow freely over the substrate during application, ensuring that it covers all voids created in the surface itself. Thus, wettability can be defined as "the ability of a liquid to spread on that surface under equilibrium conditions, without chemical interactions between the liquid and the solid".

In parallel, the wettability of obtained surfaces was evaluated by depositing drops of 5 µl of ethylene glycol. This allowed the evaluation

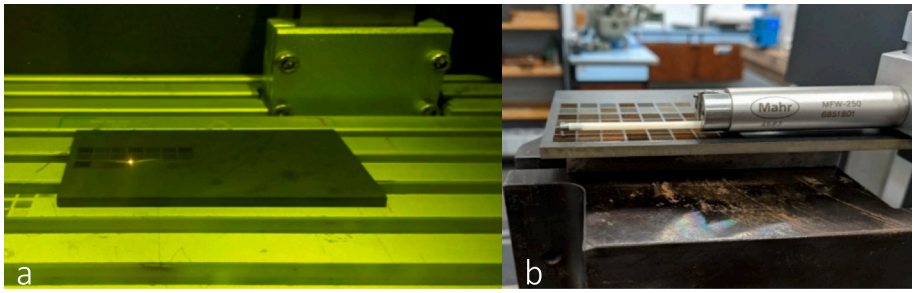

Fig. 1. A) Laser texturing of s275 carbon steel; b) evaluation of the roughness obtained in laser texturing using a roughness meter.

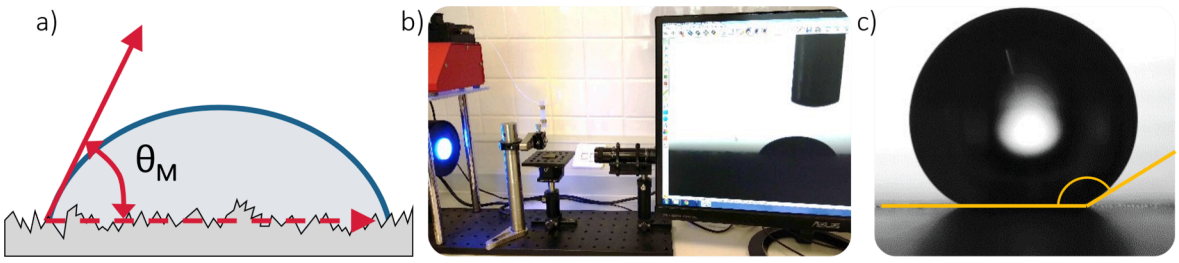

Fig. 3. A) Visual schematic of the relationship between metal surface roughness and wettability in terms of contact angle; b) scheme and set-up for wettability assessment; c) contact angle assessment by image processing.

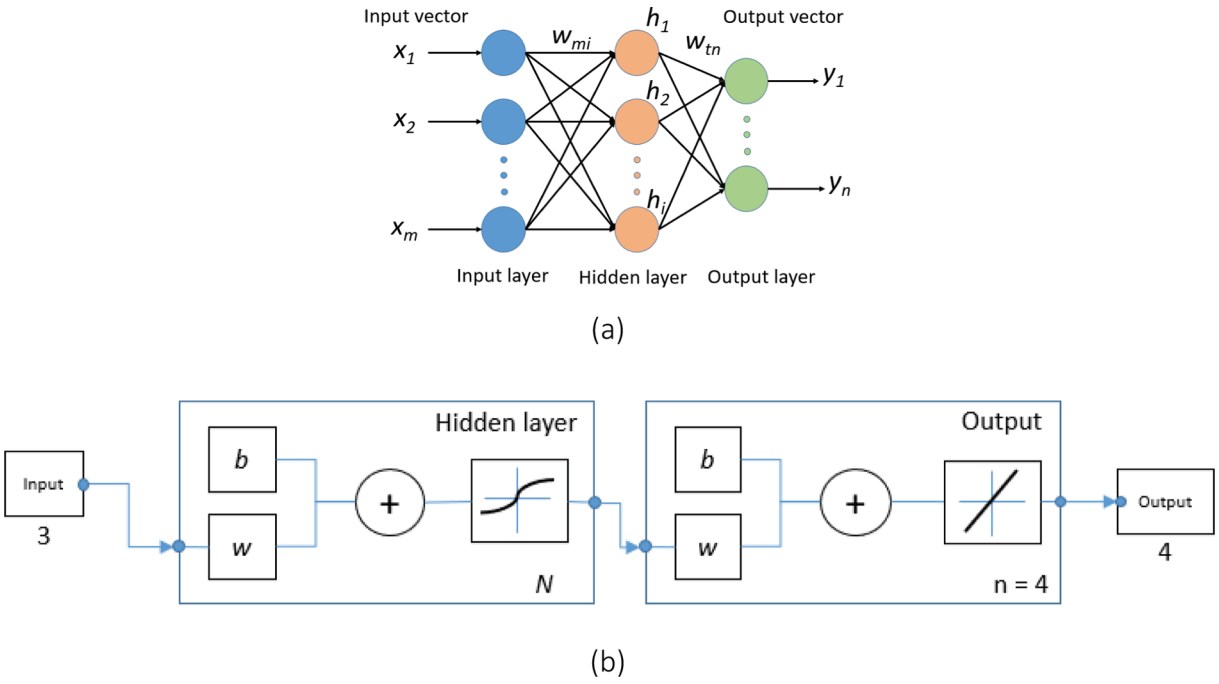

Fig. 4. (a) Typical structure of a shallow *ANN*; (b) *ANN* scheme used to perform the regression task.

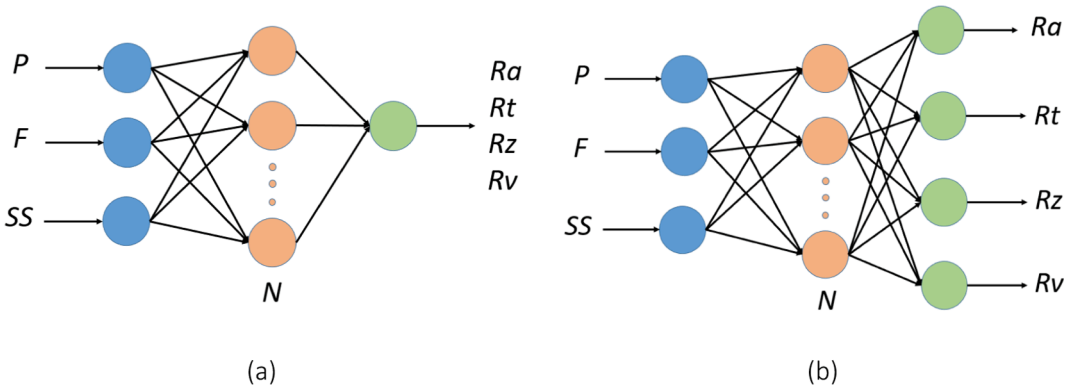

Fig. 5. ANN structure for predicting (a) one output variable (*Ra, Rt, Rz* or *Rv*) and (b) four output variables simultaneously (*Ra, Rt, Rz* or *Rv*) as a function of three input variables (*P*, *F* and *SS*).

of the contact angle parameter through image analysis. This angle is defined by the surface of a liquid in contact with the substrate surface in a state of equilibrium. Depending on the surface modification previously applied to the substrate and the ratio of the adhesive forces between the liquid and the solid and the cohesive forces of the liquid, the value of the angle obtained will vary between 0° and 90°. A phase contact angle measurement system consisted of a high-resolution CCD camera positioned on the axis that crosses the drop, while a back illumination points supplied contrast to capture the geometry (Fig. 3.b). Three contact angle measurements have been obtained to generate a mean value with

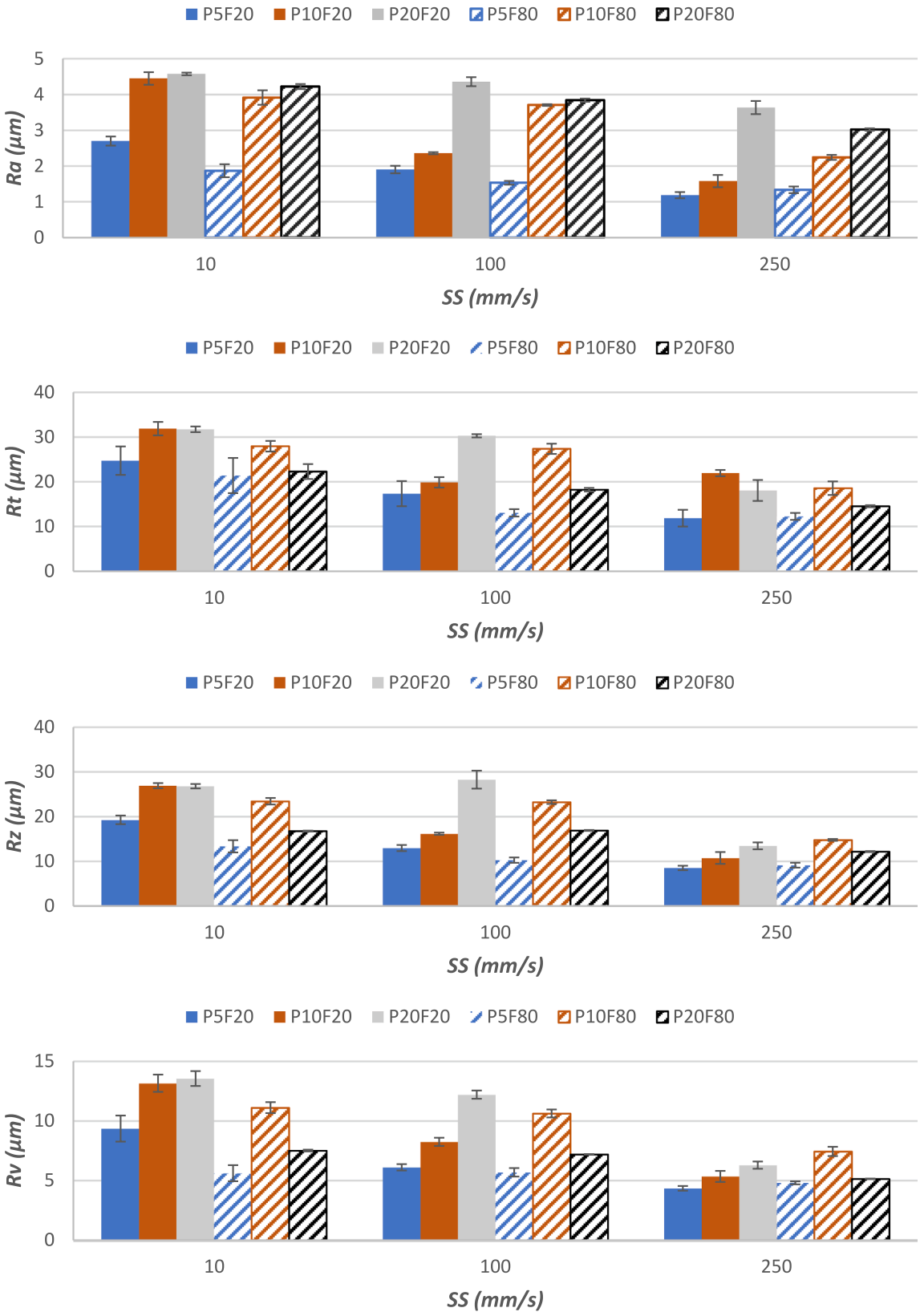

Fig. 6. Experimental results obtained in the evaluation of roughness profiles in laser texturing tests.

deviations close to 0.1° (Fig. 3.c). After laser treatment, the sample surfaces were characterized using scanning electron microscopy (SEM) using a Hitachi VP-SEM SU1510 equipment.

Once the experimental results were obtained, a statistical analysis was conducted. First, an approximation of the results obtained to predictive models based on response surfaces was performed. The use of response surface methodology (*RSM*) sets up an empirical model based on multiple linear regression [50,51]. Using this methodology, an

Table 3
Experimental results corresponding to the roughness evaluation for the experimental design.

Power (W)	Frequency (kHz)	Ed (J/cm²)	Sweep Speed (mm/s)	Ra (μm)	Deviation	Rt (μm)	Deviation	Rz (μm)	Deviation	Rv (μm)	Deviation
5	20	8.84	10	2.70	0.13	24.72	3.18	19.25	0.97	9.35	1.09
5	20	8.84	100	1.90	0.10	17.34	2.81	12.94	0.69	6.10	0.27
5	20	8.84	250	1.19	0.09	11.85	1.87	8.48	0.50	4.33	0.20
5	80	2.21	10	1.87	0.18	21.39	3.94	13.33	1.37	5.60	0.67
5	80	2.21	100	1.53	0.05	13.05	0.82	10.24	0.60	5.68	0.36
5	80	2.21	250	1.34	0.09	12.25	0.78	9.11	0.55	4.79	0.13
10	20	17.68	10	4.45	0.18	31.88	1.50	26.89	0.57	13.15	0.72
10	20	17.68	100	2.36	0.03	19.87	1.17	16.14	0.25	8.23	0.34
10	20	17.68	250	1.58	0.17	21.94	0.70	10.72	1.33	5.33	0.46
10	80	4.42	10	3.92	0.20	27.95	1.19	23.41	0.73	11.10	0.46
10	80	4.42	100	3.71	0.02	27.37	1.14	23.21	0.40	10.61	0.33
10	80	4.42	250	2.24	0.07	18.56	1.52	14.76	0.20	7.43	0.39
20	20	35.37	10	4.58	0.04	31.73	0.63	26.77	0.49	13.54	0.62
20	20	35.37	100	4.36	0.13	30.28	0.36	28.24	2.01	12.19	0.35
20	20	35.37	250	3.64	0.18	18.05	2.34	13.43	0.77	6.28	0.30
20	80	8.84	10	4.22	0.07	22.28	1.67	16.74	0.53	7.50	0.07
20	80	8.84	100	3.84	0.04	18.22	0.40	16.88	0.65	7.19	0.32
20	80	8.84	250	3.02	0.03	14.53	0.23	12.16	0.75	5.14	0.26

ANOVA analysis was carried out to obtain a series of contour plots or response surfaces. A second order polynomial equation was used to obtain these response surfaces, as described in equation (1). This type of mathematical model is widely used in the study of nonconventional machining processes to relate the defects studied to the machining parameters selected [31,52].

$$Y = C_0 + \sum_{i=1}^{k} C_i x_i + \sum_{i=1}^{k} C_{ii} x_i^2 + \sum_{i<j}^{k} C_{ij} x_i x_j + \varepsilon \quad (1)$$

Y corresponds to the expected response, in this case the mean surface roughness (*Ra*); x_i are the parameters used in the study; C_0, C_i, C_{ii}, C_{ij}, the regression coefficients; and ε the random error of the model. On the other hand, a supervised shallow Artificial Neural Network (*ANN*) was used to obtain a regression model of the experimental data. Fig. 4.a shows the typical structure of this *ANN*, characterised by using only one hidden layer [36]. In this work, a feedforward *ANN* with three input variables (*P*, *F* and *SS*) and four output variables (*Ra, Rt, Rz* and *Rv*) was used. For this purpose, the Matlab Neural Network Toolbox library and the Simulink virtual programming environments have been used. Fig. 4.b shows the two-layer feedforward network with sigmoid hidden neurons and linear output neurons used to perform the regression task. The Levenberg-Marquardt algorithm was used for training the *ANN* because it is suitable for fast training in small data sets. The 80% of the dataset were used in the training step. The remaining 20% was used to prove that the network is generalising and to stop training before overfitting.

First, an analysis of the best number of neurons (*N*) for the design of the ANN was carried out, to avoid underfitting and overfitting. This analysis was performed individually for each of the output variables (*Ra, Rt, Rz* and *Rv*), using an ANN with three input variables and only one output variable (Fig. 5.a). This ANN was tested for $N = 1$ to twenty. The Root Mean Square Error (*RMSE*) and the Mean Squared Error (*MSE*) were used as ANN performance parameter (Equation (2)). In Equation (3), $\hat{y}_t$ are the predicted values, y_t the experimental values and *T* the number of observations. The optimal number of neurons (N_{opt}) selected was the one that resulted in a minor *RMSE* of the four output variables, individually considered. The final ANN, considering all the output variables simultaneously was trained for several hidden layers equal to N_{opt} (Fig. 5.b). Since the used variables are at different scales, a normalization of their values (from 0 to 1) has been performed in this second step, to achieve a better ANN behaviour (Equation (2)). In Equation (3), Y_{norm} is the normalized value (from 0 to 1) of the variable *Y* (*Ra, Rt, Rz* and *Rv*); max*(Y)* and min*(Y)* are the maximum and minimum value of *Y* in the data set, respectively.

$$RMSE = \sqrt{MSE} = \sqrt{\frac{\sum_{t=1}^{T} (\hat{y}_t - y_t)^2}{T}} \quad (2)$$

$$Y_{norm} = \frac{Y - \min(Y)}{\max(Y) - \min(Y)} \quad (3)$$

3. Results

Results corresponding to the evaluation of the roughness generated in the different laser texturing tests are shown in Fig. 6. The graph shows the mean value obtained for each bar for the four study parameters (Ra, Rt, Rz and Rv). For each parameter, the whisker diagram expresses the standard deviation of the results obtained. In parallel, the experimental results obtained in terms of surface quality are shown in Table 3.

Note that the trends seen in the four study parameters are similar, suggesting homogeneity in the surface obtained with minor variation in texture. This observation is confirmed by the deviations found in the surface quality results, with maximum deviations of 0.2 μm for *Ra*, 3.9 μm for *Rt*, 2.0 μm for *Rz*, and 1.1 μm for *Rv*.

On the other hand, a general decreasing trend has been observed in the increase of *SS* parameter for most of the results obtained in the four study parameters. The maximum values were obtained with a scanning speed of ten mm/s, which corresponds to a longer exposure time of the metallic alloy surface to the laser beam [53,54]. As this parameter increases, i.e., the exposure decreases, the laser's penetration ability produces less rough texture. This is especially noticeable in the *Rv* parameter [21]. For the three established powers (5 W, 10 W and 20 W), the valley value obtained on the evaluated surface decreases from 9.35 μm to 4.33 μm, from 13.15 μm to 5.33 μm, and from 13.54 μm to 6.28 μm, respectively, when increasing the *SS* parameter from ten mm/s to 250 mm/s for a fixed frequency of 20 kHz. Increasing the frequency to 80 kHz reduces the surface roughness obtained. However, at 80 kHz the roughness trends are not as defined, possibly indicating that the energy density is not sufficient to produce a homogeneous texture. This may result in poorly defined surfaces, particularly at high scanning speeds, which would reduce the final roughness [55].

Similarly, higher laser beam power increases its penetration ability, allowing for a larger volume of material to be locally melted [56]. This generates a more melted material removal for the three levels of scan speed, producing a more defined pattern, as is shown in Fig. 7.a. For the same power (20 W) and frequency (20 kHz), the effect of speed on the type of surface obtained can be seen. This can be better seen by the energy density parameter (*Ed*), which expresses the energy deposited per unit area and can be related to the ratio between the head

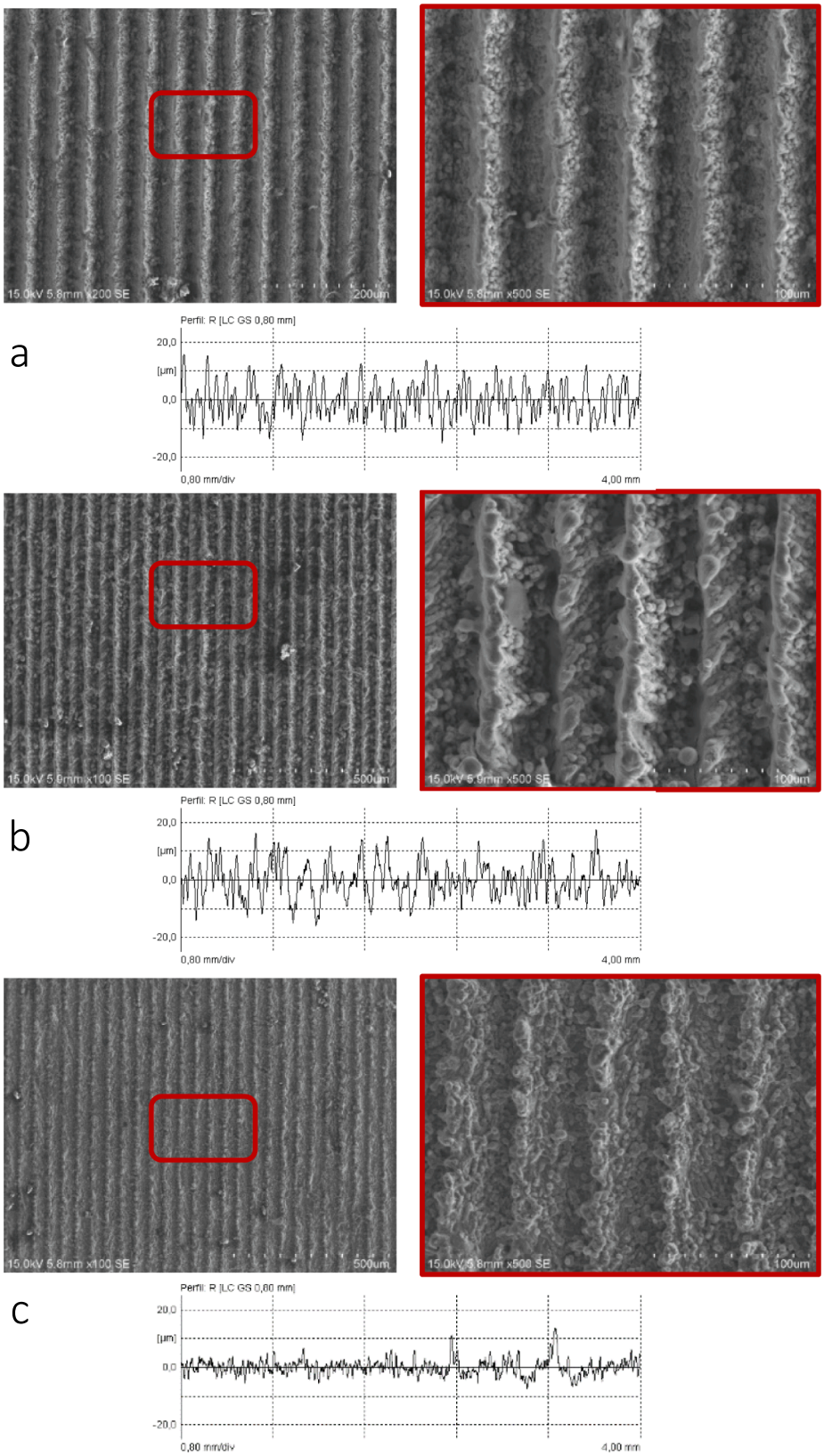

Fig. 7. Visual evaluation by SEM microscopy of the surfaces obtained by laser texturing and their corresponding roughness profile for a power of 20 W and a frequency of 20 kHz and a scanning speed of: a ten mm/s; b) 100 mm/s; c) 250 mm/s.

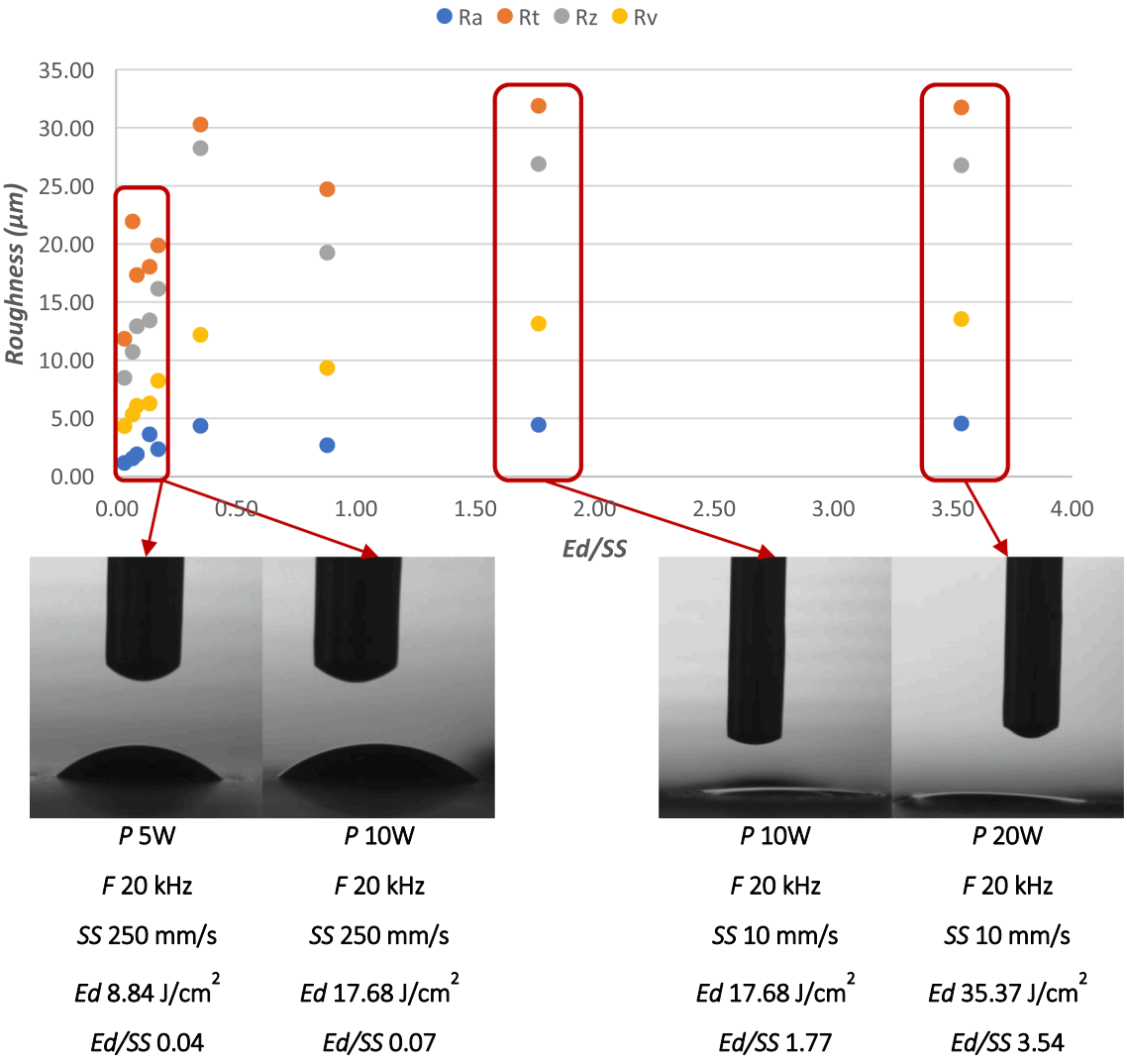

Fig. 8. Evolution of roughness as a function of four output variables (*Ra*, *Rt*, *Rz*, *Rv*) and their relationship with the energy density applied in each texturing test and the type of wettability generated on the modified surface.

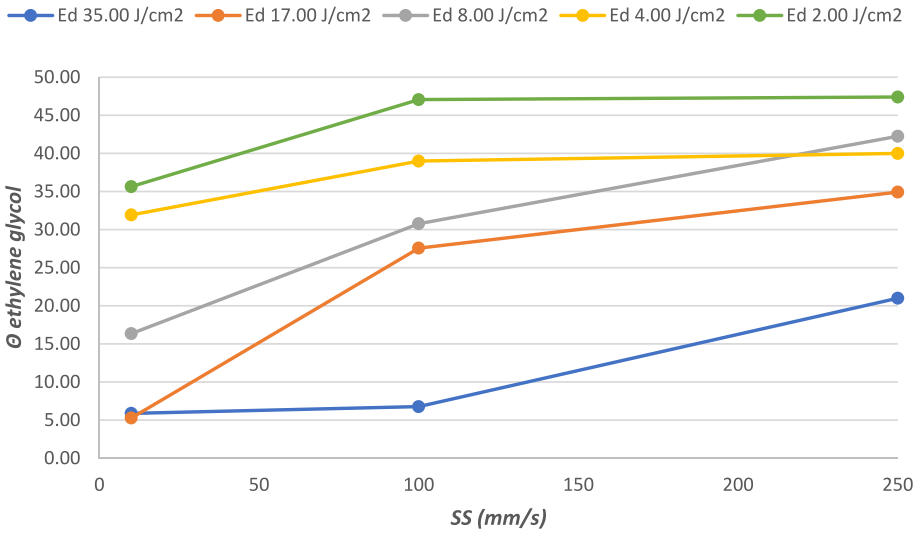

Fig. 9. Influence of the scanning speed parameter on the wettability obtained by contact angle evaluation for different laser beam energy densities.

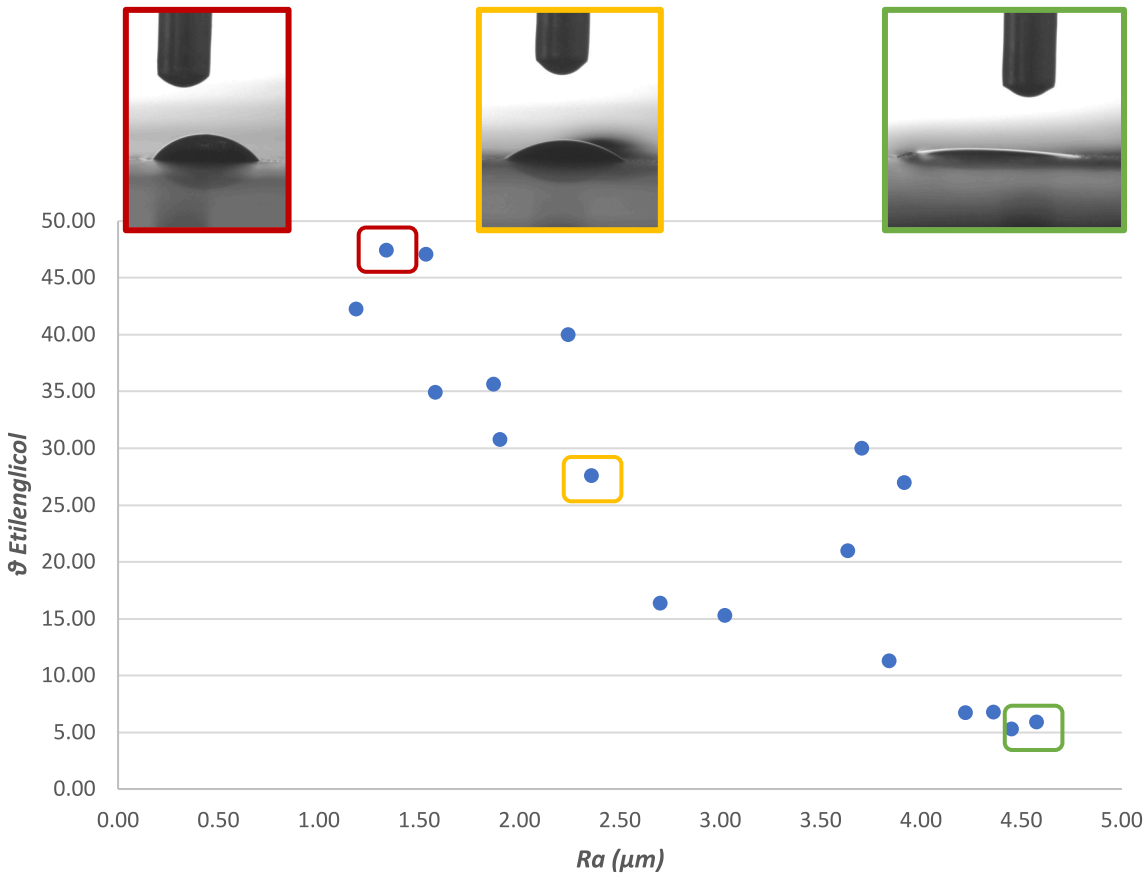

Fig. 10. Relationship between the roughness results obtained in terms of Ra and the wettability of carbon steel in terms of contact angle.

Table 4
ANOVA analysis conducted on the four evaluated roughness parameters.

Source	DF	Adj SS	Adj MS	F-Value	P-Value
Ra					
Power (W)	1.00	14.32	14.32	47.01	0.00
Frequency (kHz)	1.00	0.06	0.06	0.18	0.68
Scanning Speed (mm/s)	1.00	6.16	6.16	20.23	0.00
Error	9.00	2.74	0.30		
Total	17.00	24.03			
Rt					
Power (W)	1.00	97.08	97.08	8.97	0.02
Frequency (kHz)	1.00	63.62	63.62	5.88	0.04
Scanning Speed (mm/s)	1.00	325.57	325.57	30.07	0.00
Error	9.00	97.43	10.83		
Total	17.00	725.94			
Rz					
Power (W)	1.00	135.30	135.30	10.80	0.01
Frequency (kHz)	1.00	29.67	29.67	2.37	0.16
Scanning Speed (mm/s)	1.00	277.89	277.89	22.19	0.00
Error	9.00	112.73	12.53		
Total	17.00	695.90			
Rv					
Power (W)	1.00	20.02	20.02	10.21	0,01
Frequency (kHz)	1.00	10.02	10.02	5.11	0.05
Scanning Speed (mm/s)	1.00	61.97	61.97	31.61	0.00
Error	9.00	17.64	1.96		
Total	17.00	151.14			

displacement speed and the type of texture obtained [57]. However, the evaluation of roughness was related to the texturing parameters and not to the Ed parameter, because different power and frequency values can produce the same energy density value. In this study, the direct relationship between laser processing parameters, power and frequency, and the resulting texture geometry has been chosen over the Ed commonly used in laser studies. The focus is on understanding the individual influence of these parameters. Nevertheless, the energy per unit area, Ed, stays as a useful parameter to justify effects such as ablation or fusion, as mentioned earlier.

In Fig. 7 it can be observed that the ratio between energy density and *SS* parameter decreases, minimising the amount of energy deposited on the surface in an instant of time. This produces a reduction in laser penetration and in the volume of evaporated material, resulting in a decrease in the four roughness parameters, in good agreement with [58].

This is of great interest for the generation of hydrophobic surfaces [59]. By reducing the ratio between *Ed* and *SS*, a surface modification of the metal can be seen, generating a less rough and homogeneous surface, which may indicate a reduction in its surface activation, allowing a hydrophobic character to be achieved [60].

Fig. 8 shows the study parameters and their relationship with the *Ed/SS* ratio. The results obtained are in good agreement with what was previously shown, where a high ratio indicates a lower displacement speed for a fixed energy density, stabilising the final roughness obtained in the texture. Instead, extremely low ratios produce large variations in the roughness of the obtained texture [61].

For a fixed energy density, decreasing the exposure time to the laser beam by increasing the displacement speed modifies the type of texture obtained, as can be seen in the roughness profiles obtained in Fig. 8. For example, for a power of 20 W and a frequency of 20 kHz, equivalent to an energy density of 35.37 J/cm^2, similar roughness profiles were obtained for a speed of ten mm/s (Fig. 7.a) and a speed of 100 mm/s (Fig. 7.b). This can also be observed in Fig. 4.d, where the trends for the *Rv* parameter are very similar when increasing the *SS* parameter from ten mm/s to 100 mm/s, regardless of the established power and frequency.

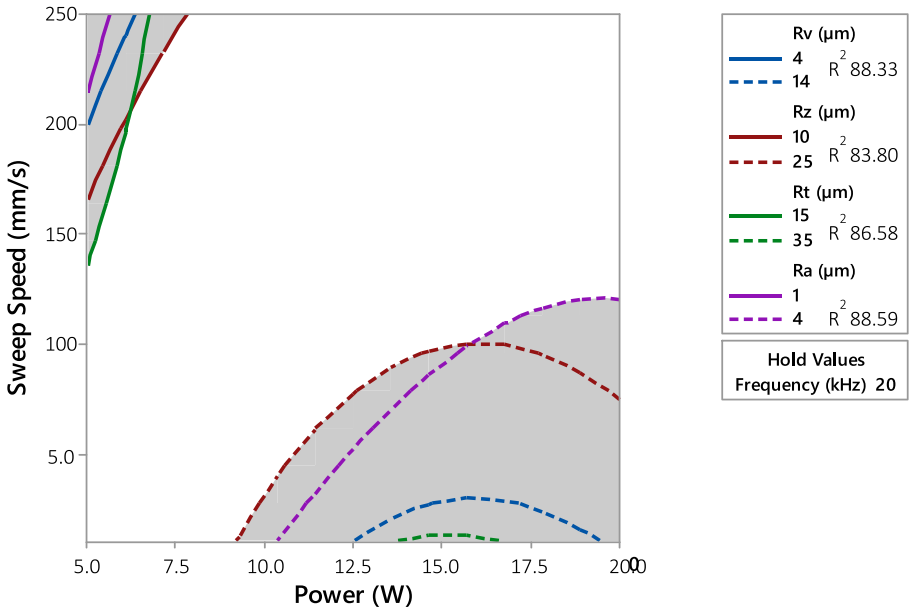

Fig. 11. Overlay contour plots obtained from the four responses surface models to find common regions.

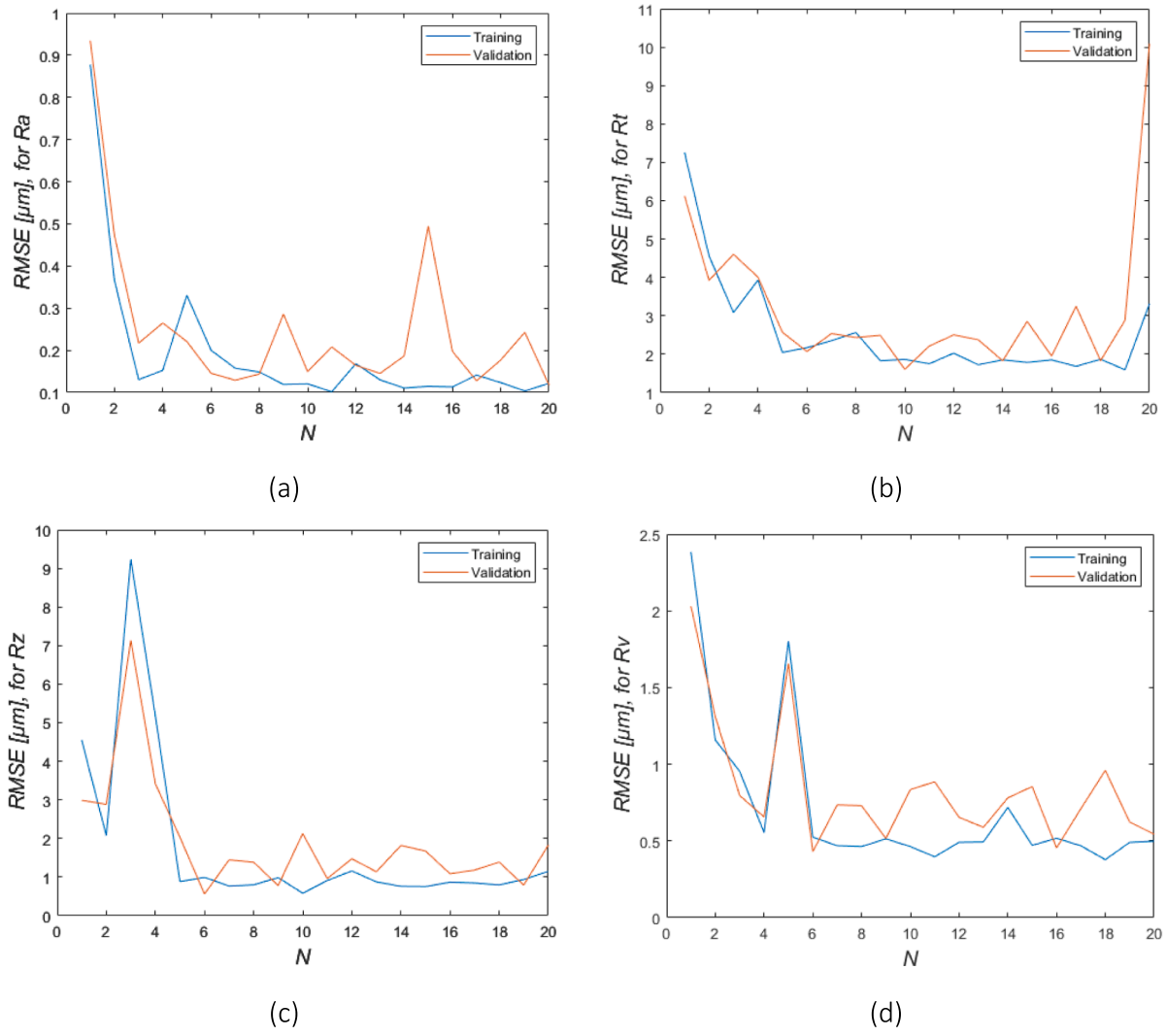

Fig. 12. *RMSE* as a function of *N*, for (a) *Ra*, (b) *Rt*, (c) *Rz* and (d) *Rv*.

Table 5
Minimum values of *RMSE* in the training and validation phases.

Output variable	*N*	*RMSE*- training phase [μm]	*RMSE*- validation phase [μm]
Ra	10	0.12	0.15
Rt	10	1.87	1.60
Rz	6	0.99	0.56
Rv	6	0.52	0.43

On the contrary, when increasing the speed to 250 mm/s (Fig. 7.c), the amount of energy developed for texturing is minimal for the same time interval, obtaining the minimum roughness values in the four study parameters.

Stabilisation is seen in all four study parameters from an approximate ratio of 1.5 (Ed/SS). This suggests that, for fixed power and frequency, reducing the speed does not increase roughness, which could mean that the laser does not have enough energy to remove more material and create deeper and more defined channels [12].

To obtain a more pronounced texture, a higher energy density would be needed. Regarding the type of surface obtained, it could be said that ratios greater than 1.5 between energy density and head speed produce superhydrophilic surfaces (Contact angles close to 0°, [62]), while ratios that tend to zero generate hydrophilic surfaces (Contac angles less than 90°) with lower surface activation [63,64]. Wetting tests with ethylene glycol have confirmed this relationship, as the contact angle has varied significantly depending on the ratio between energy density and displacement speed (Fig. 9). This agrees with the results obtained in [65]. In their study, they perform wettability tests by depositing drops of water and ethylene glycol. The authors establish a relationship between roughness and wettability. Varying the roughness by surface treatment increases the surface free energy. This implies a significant variation in the contact angles for both liquids.

The relationship between energy density (*Ed*) and scan speed (*SS*) is a key factor in the wettability of the obtained surface. It has been seen that a higher *SS* parameter increases the contact angle, regardless of the applied energy density. This effect is due to less energy being deposited in an instant, which is related to a reduction in the obtained roughness and, therefore, a minimisation of surface activation [66,67]. Similar contact angle values were obtained for ethylene glycols in the study carried out at [68]. The influence of surface treatment by increasing the roughness of the test material reduces the contact angle values from 49° to 8°.

On the other hand, a higher energy density applied produces a higher roughness on the surface. This implies that the liquid can expand more easily and impregnate a larger area, resulting in a reduction in the contact angle.

Values of Ed between eight J/cm^2 and thirty-five J/cm^2 lead to an increase in the contact angle, especially for values between ten and 100 mm/s. In contrast, lower values of energy density only change the surface at scan speeds below 100 mm/s. Above these values, the laser beam hardly changes the surface, or the roughness obtained, resulting in the same type of hydrophilic surface. This occurs similarly to the previously exposed roughness obtained [3].

In addition, it has been seen that superhydrophilic surfaces can be obtained by minimising the scan speed. This is also due to the reduction of the laser beam frequency, which increases the energy density for texturing. In contrast, high scan speeds, and an increase in frequency, result in minimal laser interaction with the surface. This generates a reduction in roughness and produces a reduction in the surface activation of steel, increasing the contact angle.

According to the Wenzel's theory, the contact area of rough surface was expanded promoting the spreading of liquid on the solid surface and the absolute wetting state was thus achieved. When a given liquid was dropped on a rough surface, the apparent contact angle θ was defined as follows: $\cos\theta_f = r\cos\theta_s$, wheres θ_s was the intrinsic contact angle, and r was the ratio of actual one to the projection area. The increase of surface roughness would make the hydrophobic surface become more hydrophilic. A similar behaviour was observed in the results obtained in [69]. To evaluate the wettability of the surface obtained after laser texturing, drops of water and ethylene glycol were deposited. Both liquids showed a reduction in their contact angles, increasing the roughness of the texture obtained and the surface free energy. This is shown in Fig. 10. It shows the relationship between the results obtained for the roughness parameter Ra and the wettability in terms of contact angles for the ethylene glycol droplets. A decreasing behaviour of the contact angle is confirmed with increasing roughness values, thus improving the wettability of the surface obtained after laser texturing.

To verify the influence of input parameters on output variables (*Ra*, *Rz*, *Rt*, *Rv*), an ANOVA analysis (Table 4) was carried out, confirming previous results. In general, for all four studied parameters, the *SS* and *P* parameters were found to be statistically more influential, with p-values below 0.05, showing their statistical significance [14]. However, for the *Ra* parameter, the displacement speed was found to be the most influential parameter with higher *F* value. This is consistent with the previously described relationship between the ratio of energy density and displacement speed and the type of surface generated.

Based on these results, a first predictive model was developed based on a response surface. This model allows experimental results to be approximated to a second order polynomial with factor interaction. Fig. 11 shows the superposition of contour diagrams related to the four outputs variables for the two most relevant parameters (*P* and *SS*).

To observe the common regions in both output variables in relation to the experimental results and the type of surface to be obtained (hydrophilic or superhydrophilic), the relationship between surface activation and controlled roughness in a metallic alloy is confirmed. The obtained models allow to set up a common region that minimises the results of the four study variables. Hydrophilic surfaces with low roughness values can be achieved with a power of 5 W and a speed of 250 mm/s, regardless of the established pulse rate. In contrast, by increasing the energy density ratio in relation to speed, through an increase in power and a speed of 10 mm/s, the highest roughness values and a superhydrophilic surface are obtained.

It is important to highlight the crucial role of the *SS* parameter, especially in relation to the *Rt* and *Rv* parameters. These parameters are related to the depth of the channels generated in texturing, which allows the total expansion of the deposited liquid.

It can be seen that the maximum values of these parameters can be reached in a range of 10 W to 20 W as long as the speed is at a minimum of ten mm/s. This guarantees maximum interaction of the laser beam with the metal surface and eliminates the largest amount of material per pass, reaching a stable maximum regardless of the power.

An alternative to outcome prediction is the use of predictive models based on neural networks to achieve a better fit. The correct selection of neurons to optimise the final result and establish a score prediction is shown below [70].

Fig. 12 shows the root mean square error (RMSE) as a function of the number of neurons considered in the hidden layer, for the training and validation phases, according to the *ANN* scheme shown in Fig. 12.a.

As it can be seen in Fig. 12, the *RMSE* stabilizes between $N = 6$ and $N = 10$ for all output variables. Table 5 shows the number of neurons in the hidden layer (*N*) that give rise to a minimum value of the sum of *RMSE* in the training and validation phases. For *Ra* and *Rt*, the minimum value was obtained for $N = 10$. Although the best *N* for *Rz* and *Rv* was reached for $N = 6$, the *RMSE* for $N = 10$ was remarkably close. Therefore, the best value selected to test the global ANN, considering the four outputs simultaneously (Fig. 12.b), was $N_{opt} = 10$.

Fig. 13 shows the regression results of the *ANN* (N = 10) for every output variable, individually considered (as shown in Fig. 5.a), for the data used in the training and validation phase, as well as for the full set of data. Table 6 shows the results for the adjusted R^2 for the training and validation phase, and for the full set of data.

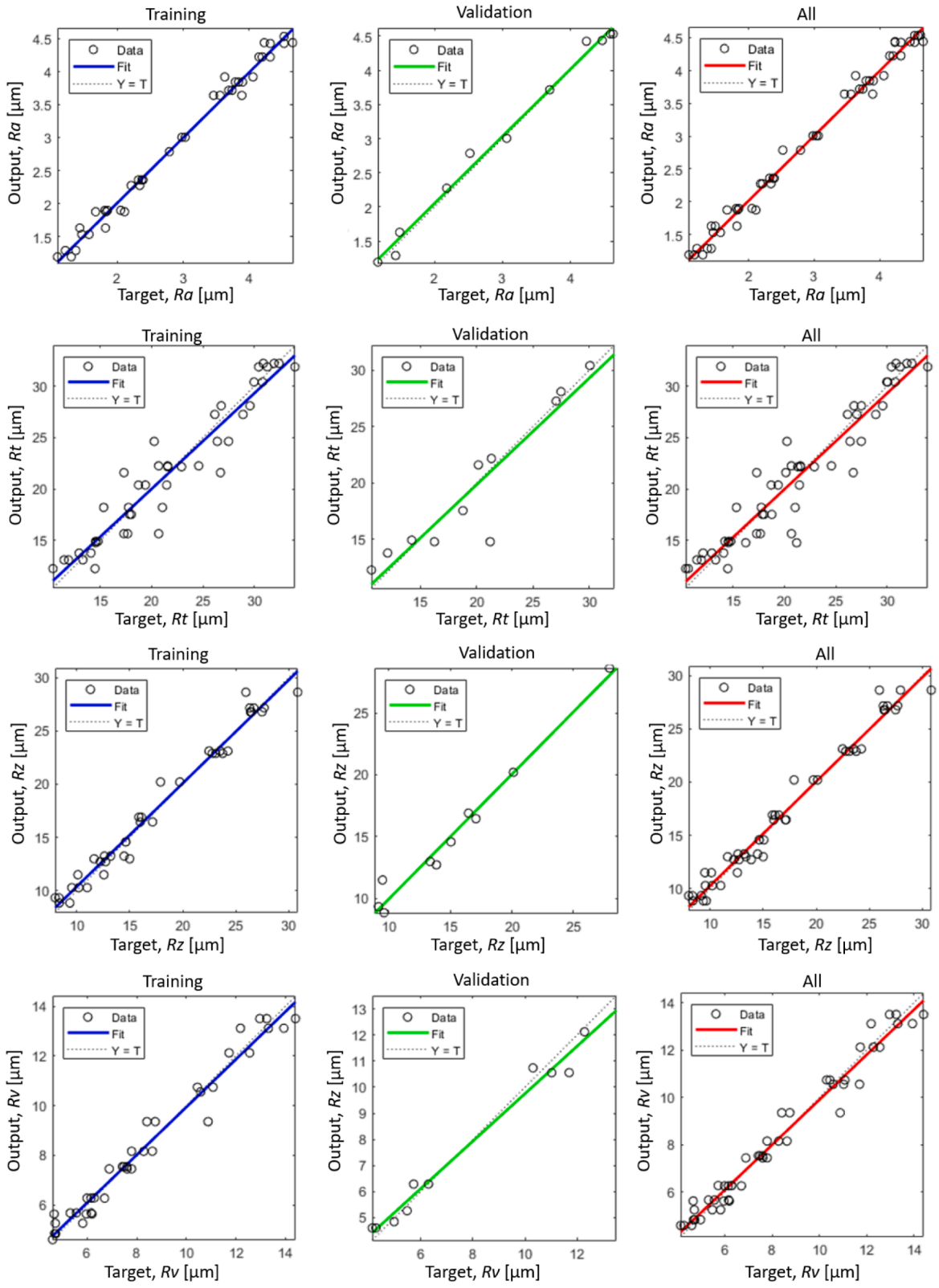

Fig. 13. *ANN* regression results ($N = 10$) for the training and validation phase, and considering all data (for every output variable).

The *ANN* shown in Fig. 5.b, which includes the four output variables (*Ra, Rt, Rz* and *Rv*) simultaneously, was tested for $N = 10$. Fig. 14.a shows the results for the ANN training performance. The number of iterations (epochs) performed was fifteen. The *MSE* was progressively reduced, both in the training and the validation phases. The best validation performance was obtained for the epoch nine, with a *MSE* close to $7{\cdot}10^{-3}$.

Fig. 14.b shows the *ANN* error histogram. Most of the results (around

Table 6
Adjusted R^2 for every output variable individually considered.

Output variable	training	validation	All	RSM
Ra	0.987	0.986	0.988	0.8859
Rt	0.905	0.810	0.899	0.8658
Rz	0.974	0.962	0.975	0.8380
Rv	0.966	0.962	0.968	0.8833

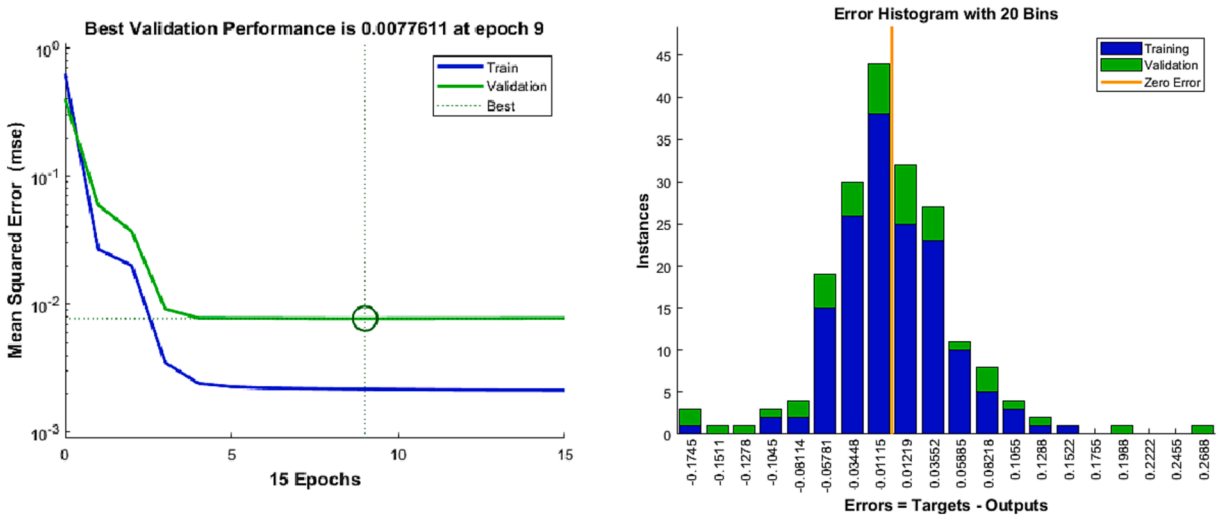

Fig. 14. (a) *ANN* training performance; (b) *ANN* error histogram.

Table 7
RMSE in the training and validation phases ($N = 10$, normalised values).

	***RMSE* (Training)**	***RMSE* (Validation)**
All data set	0.046	0.088
Ra	0.035	0.037
Rt	0.066	0.130
Rz	0.031	0.075
Rv	0.045	0.083

85%) have shown an error value of less than ± 5%. Only the 4% of the dataset has shown an error between 15% and 27%.

Table 7 shows the *RMSE* for the training and validation phases, for all data sets and for every input variable. The *RMSE* has been calculated for the normalised data (from 0 to 1). The dataset shows a reasonable value for the *RMSE*, between 3.1% (*Rz*, training phase) and 13% (*Rt*, validation phase).

Fig. 15 shows the *ANN* regression results for the training and validation phases and for all data set. Table 8 shows the results for the adjusted R^2 for the training and validation phase, and for the full set of data ($N = 10$, normalised data).

Finally, the error of the results obtained is shown in Fig. 16. In general, the use of neural networks as a predictive model offers a smaller difference between the predicted and obtained results. Both the *RSM* and *ANN* models give close predictions with good fits. It should be noted that for the *Ra* parameter, the differences obtained by *ANN* are less than 0.3 μm. Neural network prediction models results in better results, with the advantage that the model predicts the behaviour of all four variables studied. The *RSM* method, on the other hand, can only produce an individual model for each variable without proving a relationship with the other output variables. In summary, the use of neural networks as a predictive model has proven to be more correct and efficient than *RSM*, allowing a better understanding and prediction of the relationship between input parameters and output responses [71,72].

ANN models have proven to be highly efficient in empirical modelling and prediction, especially for non-linear systems. Their predictive capabilities far exceed those of *RSM* models. Unlike *RSM* models, which are limited to modelling quadratic relationships between input and

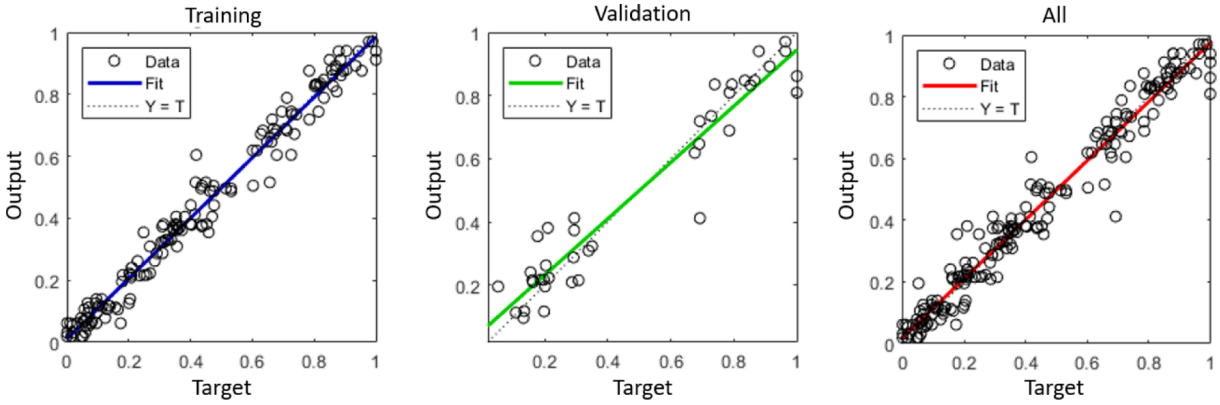

Fig. 15. *ANN* regression results ($N = 10$, normalised data).

Table 8
Adjusted R^2 for every output variable.

Output variable	Training	Validation	All	RSM
Ra	0.988	0.937	0.987	0.8859
Rt	0.937	0.733	0.907	0.8658
Rz	0.986	0.915	0.974	0.8380
Rv	0.959	0.922	0.958	0.8833

output variables, *ANN* models excel at handling complex and non-linear relationships. Furthermore, *ANN* models could learn from large data sets and generalise effectively to new data, whereas RSM models require numerous experiments to achieve accurate predictions. In addition, *ANN* are better at dealing with missing and noisy data than *RSM* models [73]. This is corroborated in the results obtained, where the fit obtained by response surface model prediction is lower than that obtained by neural network prediction. This is reflected in greater variations with respect to the real value to be obtained.

4. Conclusions

This study investigated the effects of scanning speed (*SS*), Power (*P*), frequency (*F*) and energy density (*Ed*) as laser texturing parameters on the surface properties of a S275 carbon steel, for roughness parameters (*Ra*, *Rt*, *Rz* and *Rv*) and hydrophobicity. The results show that slower scanning speeds lead to increased roughness and higher asperity values. This increases its surface activation in terms of wettability.

The relationship between energy density and scanning speed was found to affect the hydrophobicity of the surface, with superhydrophilic surfaces obtained at *Ed/SS* ratios greater than 1.5 and hydrophilic surfaces obtained when this ratio approached zero. This confirms the direct relationship between texturing parameters, generated roughness, and wettability in terms of contact angle. The correct choice of texturing parameters makes it possible to reach a superhydrophilic state with angles close to 0° as the roughness is increased. This relationship between roughness and wettability is linear. Thus, an increase in roughness reduces the value of the contact angle.

Increasing the scanning speed reduced surface activation and roughness, which in turn increased the contact angle. In contrast, increasing the energy density resulted in increased roughness and decreased contact angle. This allows greater interaction between the laser beam and the surface being textured, increasing the volume of material evaporated and achieving greater precision in the texturing pattern.

This research has investigated the effectiveness of response surface

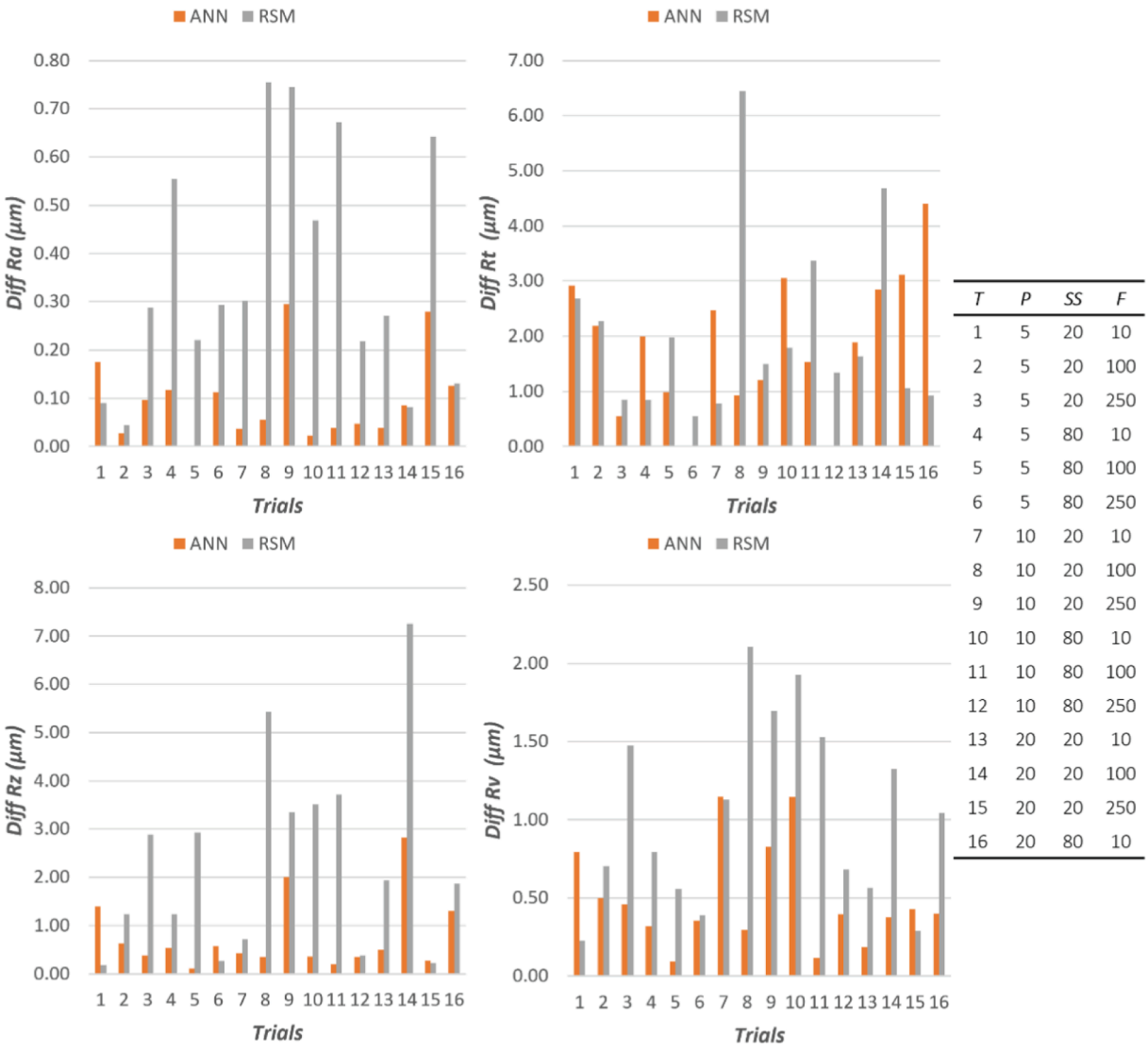

T	P	SS	F
1	5	20	10
2	5	20	100
3	5	20	250
4	5	80	10
5	5	80	100
6	5	80	250
7	10	20	10
8	10	20	100
9	10	20	250
10	10	80	10
11	10	80	100
12	10	80	250
13	20	20	10
14	20	20	100
15	20	20	250
16	20	80	10

Fig. 16. Differences in absolute values between the results obtained by the predictive response surface models and neural networks with respect to the experimental results for the variables: a) *Ra*; b) *Rt*; c) *Rz*; d) *Rv*.

methodology (RSM) and artificial neural network (ANN) modelling techniques in the prediction of surface roughness. Both approaches produced models with high levels of accuracy (over 85%). However, ANN models consistently outperformed RSM models, achieving high levels of accuracy more than 90% in the majority of cases. In addition, the ANN model is able to respond to multiple output responses simultaneously. In addition, a model was obtained using *ANN* that included all four surface parameters, allowing correct predictions with less than 0.3 μm difference in *Ra* compared to *RSM* models that could only predict a single variable with a higher fitting error.

In conclusion, the results prove the importance of considering both scanning speed and energy density in controlling surface properties, with slower scanning speeds and higher energy densities leading to increased roughness and decreased hydrophilicity. It is possible to modify the behaviour of a carbon steel for future applications, such as the use of adhesives, increasing the wettability of the steel by increasing the roughness of the texture.

Furthermore, *ANN* modelling techniques appear to be more effective than *RSM* in predicting surface properties, particularly when multiple variables are considered simultaneously. These findings could have significant implications for a range of applications, including engineering materials and surface modification for biomaterials, among others.

CRediT authorship contribution statement

F. Bañon: Conceptualization, Data curation, Formal analysis, Investigation, Methodology, Project administration, Software, Writing – original draft. **S. Martin:** Investigation, Methodology, Supervision, Validation, Wridting – review & editing. **J.M. Vazquez-Martinez:** Supervision, Validation, Wridting – review & editing. **J. Salguero:** Supervision, Wridting – review & editing. **F.J. Trujillo:** Conceptualization, Data curation, Formal analysis, Investigation, Methodology, Project administration, Software, Wridting – review & editing.

Declaration of Competing Interest

The authors declare that they have no known competing financial interests or personal relationships that could have appeared to influence the work reported in this paper.

Data availability

No data was used for the research described in the article.

References

[1] P. Pou, J. del Val, A. Riveiro, R. Comesaña, F. Arias-González, F. Lusquiños, M. Bountinguiza, F. Quintero, J. Pou, Laser Texturing of Stainless Steel under Different Processing Atmospheres: From Superhydrophilic to Superhydrophobic Surfaces, Appl Surf Sci 475 (2019) 896–905, https://doi.org/10.1016/j.apsusc.2018.12.248.

[2] A.H. Garrido, R. González, M. Cadenas, C. Wang, F. Sadeghi, Lasers in Surface Engineering, in: Lasers in Manufacturing, Wiley, 2013, pp. 247–291.

[3] J.M. Vazquez-Martinez, J.S. Gomez, P.F.M. Ares, S.R. Fernandez-Vidal, M.B. Ponce, Effects of Laser Microtexturing on the Wetting Behavior of Ti6Al4V Alloy, Coatings 8 (2018) 7–10, https://doi.org/10.3390/coatings8040145.

[4] A.T. Tsubaki, M.A. Koten, M.J. Lucis, C. Zuhlke, N. Ianno, J.E. Shield, D. R. Alexander, Formation of Aggregated Nanoparticle Spheres through Femtosecond Laser Surface Processing, Appl Surf Sci 419 (2017) 778–787, https://doi.org/10.1016/j.apsusc.2017.05.094.

[5] A.I. Aguilar-Morales, S. Alamri, T. Kunze, A.F. Lasagni, Influence of Processing Parameters on Surface Texture Homogeneity Using Direct Laser Interference Patterning, Opt Laser Technol 107 (2018) 216–227, https://doi.org/10.1016/j.optlastec.2018.05.044.

[6] J. Vazquez Martinez, I. Del Sol Illana, P. Iglesias Victoria, J. Salguero, Assessment the Sliding Wear Behavior of Laser Microtexturing Ti6Al4V under Wet Conditions, Coatings 9 (2019) 67, https://doi.org/10.3390/coatings9020067.

[7] R. Sandeep, B. Murali Nagarajan, S. Kamlesh Kumar, S.J. Adarsh, M. Manoharan, A. Natarajan, Strategies to Improve Joint Strength of Friction Lap Welded AA7475/PPS Hybrid Joint with Surface Pre-Treatment on AA7475, Mater. Lett. 333 (2023), https://doi.org/10.1016/j.matlet.2022.133561.

[8] T. Sangu, Y. Xin, T. Hitomi, K. Kato, T. Shirai, Influence of Ball Materials on the Surface Activation Behavior of Coal Ash Particles during a Mechanochemical Process, Ceram Int (2023), https://doi.org/10.1016/j.ceramint.2023.06.219.

[9] J.P. Davim (Ed.), *Nonconventional Machining*; De Gruyter, 2022; ISBN 9783110584479.

[10] J.P. Davim, *Nontraditional Machining Processes*, in: J.P. Davim (Ed.), Springer London, London, 2013; ISBN 978-1-4471-5178-4.

[11] M. Botana-Galvín, G. Blanco, L. González-Rovira, M.A. Rodríguez, F.J. Botana, Adhesive Behaviour of Carbon Fibre Reinforced Plastic Panels Manufactured Using Woven and Unidirectional Tape after Ultraviolet Laser Surface Treatment, J. Compos. Mater. 52 (2018) 853–865, https://doi.org/10.1177/0021998317718614.

[12] Z. Yuan Jia, T. Ye, J. Wei Ma, X. Kun Cao, W. Liu, W. Jiang Yu, J. Gao, Effect of Process Parameters on the Hardness of Laser Surface Textured 5A06 Aluminum Alloy, J Mater Eng Perform 30 (2021) 5858–5867, https://doi.org/10.1007/s11665-021-05840-y.

[13] D. Przestacki, R. Majchrowski, L. Marciniak-Podsadna, Experimental Research of Surface Roughness and Surface Texture after Laser Cladding, Appl Surf Sci 388 (2015) 420–423, https://doi.org/10.1016/j.apsusc.2015.12.093.

[14] A. Marques, A. Cunha, S. Faria, F.S. Silva, O. Carvalho, Predictive Models on the Influence of Laser Texturing Parameters on the Inconel 718 Surface by Using Nd:YVO4 Laser, Opt Laser Technol 154 (2022), https://doi.org/10.1016/j.optlastec.2022.108320.

[15] K. Ganesa Balamurugan, Effect of Laser Surface Texturing Parameters on the Texture Formation in Pure Magnesium Substrate, Mater. Today:. Proc. 72 (2023) 2096–2101, https://doi.org/10.1016/j.matpr.2022.08.216.

[16] J. Xiao, Y. Zhang, B. Hu, X. Liu, Z. Liang, Z. Zhao, Tribological Properties of Ti6Al4V Alloy Composite Texture Fabricated by Ultrasonic Strengthening Grinding and Laser Processing, Materials 16 (2023), https://doi.org/10.3390/ma16010355.

[17] X. Xi, Y. Pan, P. Wang, X. Fu, Effect of Laser Processing Parameters on Surface Texture of Ti6Al4V Alloy, in: Proceedings of the IOP Conference Series: Materials Science and Engineering; Institute of Physics Publishing, vol. 563, August 9 2019.

[18] J.P. Davim (Ed.), *Surface Integrity in Machining*, Springer London, London, 2010; ISBN 978-1-84882-873-5.

[19] N. Sirdeshmukh, G. Dongre, Achieving Controlled Topography and Wettability through Laser Surface Texturing of Ti6Al4V for Bioengineering Applications, Results Eng. 17 (2023), 100898, https://doi.org/10.1016/j.rineng.2023.100898.

[20] J. Lawrence, L. Li, Carbon Steel Wettability Characteristics Enhancement for Improved Enamelling Using a 1.2 KW High Power Diode Laser, Opt Lasers Eng 32 (1999) 353–365.

[21] L. Yang, Z. Deng, B. He, T. Özel, An Experimental Investigation on Laser Surface Texturing of AISI D2 Tool Steel Using Nanosecond Fiber Laser, Lasers Manuf. Mater. Process. 8 (2021) 140–156, https://doi.org/10.1007/s40516-021-00144-4.

[22] A.O. Ijaola, E.A. Bamidele, C.J. Akisin, I.T. Bello, A.T. Oyatobo, A. Abdulkareem, P. K. Farayibi, E. Asmatulu, Wettability Transition for Laser Textured Surfaces: A Comprehensive Review, Surf. Interfaces 21 (2020), 100802, https://doi.org/10.1016/j.surfin.2020.100802.

[23] X. Sourd, R. Zitoune, L. Crouzeix, M. Coulaud, Influence of the Texturing Quality Consecutive to Abrasive Water Jet Machining on the Adhesive Properties in Mode I of 3D Woven Composite Assemblies, Composites: Part BEng 242 (2022), https://doi.org/10.1016/j.compositesb.2022.110091.

[24] X. Kong, L. Yang, H. Zhang, G. Chi, Y. Wang, Optimization of Surface Roughness in Laser-Assisted Machining of Metal Matrix Composites Using Taguchi Method, Int. J. Adv. Manuf. Technol. 89 (2017) 529–542, https://doi.org/10.1007/s00170-016-9115-1.

[25] S. Negi, S. Dhiman, R.K. Sharma, Investigating the Surface Roughness of SLS Fabricated Glass-Filled Polyamide Parts Using Response Surface Methodology, Arab. J. Sci. Eng. 39 (2014) 9161–9179, https://doi.org/10.1007/s13369-014-1434-7.

[26] K. Ninikas, J. Kechagias, K. Salonitis, The Impact of Process Parameters on Surface Roughness and Dimensional Accuracy during Co2 Laser Cutting of Pmma Thin Sheets, J. Manuf. Mater. Process. 5 (2021), https://doi.org/10.3390/jmmp5030074.

[27] K.E.C. Vidyasagar, A. Rana, D. Kalyanasundaram, Optimization of Laser Parameters for Improved Corrosion Resistance of Nitinol, Mater. Manuf. Process. (2020) 1661–1669, https://doi.org/10.1080/10426914.2020.1784926.

[28] M. Conradi, A. Kocijan, D. Klobčar, M. Godec, Influence of Laser Texturing on Microstructure, Surface and Corrosion Properties of Ti-6al-4v, Metals (Basel) 10 (2020) 1–9, https://doi.org/10.3390/met10111504.

[29] K.M. Mroczkowska, A.J. Antończak, J. Gąsiorek, The Corrosion Resistance of Aluminum Alloy Modified by Laser Radiation, Coatings 9 (2019) 1–10, https://doi.org/10.3390/coatings9100672.

[30] A. Al-Mahdy, H.R. Kotadia, M.C. Sharp, T.T. Opoz, J. Mullett, J.I. Ahuir-Torres, Effect of Surface Roughness on the Surface Texturing of 316 l Stainless Steel by Nanosecond Pulsed Laser, Lasers Manuf. Mater. Process. 10 (2023) 141–164, https://doi.org/10.1007/s40516-022-00199-x.

[31] G. Kibria, S. Chatterjee, I. Shivakoti, B. Doloi, B. Bhattacharyya, RSM Based Experimental Investigation and Analysis into Laser Surface Texturing on Titanium Using Pulsed Nd:YAG Laser. In Proceedings of the IOP Conference Series: Materials Science and Engineering; Institute of Physics Publishing, July 13 2018; Vol. 377.

[32] F. Bañon, A. Sambruno, R. Ruiz-Garcia, J. Salguero, P.F. Mayuet, Study of the Influence of Cutting Parameters on Surface Quality in AWJM Machining of Thermoplastic Matrix Composites, Proc. Manuf 41 (2019) 233–240, https://doi.org/10.1016/j.promfg.2019.07.051.

[33] J.P. Davim (Ed.), *Statistical and Computational Techniques in Manufacturing*, Springer Berlin Heidelberg, Berlin, Heidelberg, 2012, ISBN 978-3-642-25858-9.

[34] D.H. Kim, T.J.Y. Kim, X. Wang, M. Kim, Y.J. Quan, J.W. Oh, S.H. Min, H. Kim, B. Bhandari, I. Yang, et al., Smart Machining Process Using Machine Learning: A Review and Perspective on Machining Industry, Int. J. Precision Eng. Manuf. - Green Technol. 5 (2018) 555–568.

[35] A. du Preez, G.A. Oosthuizen, Machine Learning in Cutting Processes as Enabler for Smart Sustainable Manufacturing. In Proceedings of the Procedia Manufacturing; Elsevier B.V., 2019; Vol. 33, pp. 810–817.

[36] Z. Jurkovic, G. Cukor, M. Brezocnik, T. Brajkovic, A Comparison of Machine Learning Methods for Cutting Parameters Prediction in High Speed Turning Process, J. Intell. Manuf. 29 (2018) 1683–1693, https://doi.org/10.1007/s10845-016-1206-1.

[37] V. Lalwani, P. Sharma, C.I. Pruncu, D.R. Unune, Response Surface Methodology and Artificial Neural Network-Based Models for Predicting Performance of Wire Electrical Discharge Machining of Inconel 718 Alloy, J. Manuf. Mater. Process. 4 (2020), https://doi.org/10.3390/jmmp4020044.

[38] K.A. Patel, P.K. Brahmbhatt, A Comparative Study of the RSM and ANN Models for Predicting Surface Roughness in Roller Burnishing, Procedia Technol. 23 (2016) 391–397, https://doi.org/10.1016/j.protcy.2016.03.042.

[39] H. Sohrabpoor, R.T. Mousavian, M. Obeidi, I.U. Ahad, D. Brabazon, Improving Precision in the Prediction of Laser Texturing and Surface Interference of 316L Assessed by Neural Network and Adaptive Neuro-Fuzzy Inference Models, Int. J. Adv. Manuf. Technol. 104 (2019) 4571–4580, https://doi.org/10.1007/s00170-019-04291-z.

[40] S. Ray, M. Haque, T. Ahmed, T.T. Nahin, Comparison of Artificial Neural Network (ANN) and Response Surface Methodology (RSM) in Predicting the Compressive and Splitting Tensile Strength of Concrete Prepared with Glass Waste and Tin (Sn) Can Fiber, J. King Saud Univ. – Eng. Sci. (2021), https://doi.org/10.1016/j.jksues.2021.03.006.

[41] R.I.M. Asri, W.S.W. Harun, M. Samykano, N.A.C. Lah, S.A.C. Ghani, F. Tarlochan, M.R. Raza, Corrosion and Surface Modification on Biocompatible Metals: A Review, Mater. Sci. Eng. C 77 (2017) 1261–1274.

[42] T. Trzepieciński, V. Oleksik, T. Pepelnjak, S.M. Najm, I. Paniti, K. Maji, Emerging Trends in Single Point Incremental Sheet Forming of Lightweight Metals. *Metals (Basel)* 2021, *11*.

[43] A. Monden, M.G.R. Sause, S. Horn, Surface Modified Steel/Epoxy-Based CFRP Hybrid Laminates under Mode I, Mode II and Mixed-Mode Load Conditions. *ECCM 2016 - Proceeding of the 17th European Conference on Composite Materials,* **2016**.

[44] M.A.G. Silva, H. Biscaia, P. Ribeiro, On Factors Affecting CFRP-Steel Bonded Joints, Constr Build Mater 226 (2019) 360–375, https://doi.org/10.1016/j.conbuildmat.2019.06.220.

[45] P. Amend, G. Mallmann, S. Roth, R. Schmitt, M. Schmidt, Process-Structure-Property Relationship of Laser-Joined Thermoplastic Metal Hybrids, J Laser Appl 28 (2016), 022403, https://doi.org/10.2351/1.4944099.

[46] T. Ishikawa, K. Amaoka, Y. Masubuchi, T. Yamamoto, A. Yamanaka, M. Arai, J. Takahashi, Overview of Automotive Structural Composites Technology Developments in {Japan}, Compos Sci Technol 155 (2018) 221–246, https://doi.org/10.1016/j.compscitech.2017.09.015.

[47] W. Bogacz, M. Lemanowicz, M.H. Al-Rashed, D. Nakonieczny, T. Piotrowski, J. Wójcik, Impact of Roughness, Wettability and Hydrodynamic Conditions on the Incrustation on Stainless Steel Surfaces, Appl Therm Eng 112 (2017) 352–361, https://doi.org/10.1016/j.applthermaleng.2016.10.076.

[48] B. Arifvianto, Suyitno, M. Mahardika, Effect of Sandblasting and Surface Mechanical Attrition Treatment on Surface Roughness, Wettability, and Microhardness Distribution of AISI 316L, *Key Eng Mater 462–463* (**2011**) 738–743, 10.4028/www.scientific.net/KEM.462-463.738.

[49] I. Iovinella, A. Prota, C. Mazzotti, Influence of Surface Roughness on the Bond of FRP Laminates to Concrete, Constr Build Mater 40 (2013) 533–542, https://doi.org/10.1016/j.conbuildmat.2012.09.112.

[50] J. Lopes, L. Reis, D. Stefaniak, M. Freitas, P.P. Camanho, Mechanical Characterisation of CFRP-Steel Hybrid Composites, Int. J. Automotive Compos. 2 (2016) 139, https://doi.org/10.1504/IJAUTOC.2016.082071.

[51] A. Al-Mosawe, R. Al-Mahaidi, Performance of CFRP-Steel Joints Enhanced with Bi-Directional CFRP Fabric, Constr Build Mater 197 (2019) 72–82, https://doi.org/10.1016/j.conbuildmat.2018.11.235.

[52] M.C. Kong, D. Axinte, Response of Titanium Aluminide Alloy to Abrasive Waterjet Cutting: Geometrical Accuracy and Surface Integrity Issues versus Process Parameters, Proc Inst Mech Eng B J Eng Manuf 223 (2009) 19–41, https://doi.org/10.1243/09544054JEM1226.

[53] A.H.A. Lutey, L. Romoli, Surface Topography Following Pulsed Laser Texturing: Implications for Adhesion and Wettability, *Surf Topogr* **2019**, *7*, 10.1088/2051-672X/ab5c82.

[54] T. Steege, G. Bernard, P. Darm, T. Kunze, Prediction of Surface Roughness in Functional Laser Surface Texturing Utilizing Machine Learning, **2023**.

[55] A. Soveja, E. Cicală, D. Grevey, J.M. Jouvard, Optimisation of TA6V Alloy Surface Laser Texturing Using an Experimental Design Approach, Opt Lasers Eng 46 (2008) 671–678, https://doi.org/10.1016/j.optlaseng.2008.04.009.

[56] B. Mao, A. Siddaiah, Y. Liao, P.L. Menezes, Laser Surface Texturing and Related Techniques for Enhancing Tribological Performance of Engineering Materials: A Review, J Manuf Process 53 (2020) 153–173.

[57] Y. Seid Ahmed, J.M. DePaiva, F.L. Amorim, R.D. Torres, W. de Rossi, S.C. Veldhuis, Laser Surface Texturing and Characterization of Austenitic Stainless Steel for the Improvement of Its Surface Properties, 10.1007/s00170-021-07284-z/Published.

[58] L. Lazov, E. Teirumnieks, N. Angelov, E. Yankov, Modification of the Roughness of 304 Stainless Steel by Laser Surface Texturing (LST), Laser Phys. 33 (2023), https://doi.org/10.1088/1555-6611/acbb76.

[59] B.S. Yilbas, M. Khaled, N. Abu-Dheir, N. Aqeeli, S.Z. Furquan, Laser Texturing of Alumina Surface for Improved Hydrophobicity, Appl Surf Sci 286 (2013) 161–170, https://doi.org/10.1016/j.apsusc.2013.09.040.

[60] L. Gemini, M. Faucon, L. Romoli, R. Kling, High Throughput Laser Texturing of Super-Hydrophobic Surfaces on Steel. In Proceedings of the Laser-based Micro- and Nanoprocessing XI; SPIE, February 17 2017; Vol. 10092, p. 100921G.

[61] J.M.V. Martínez, J.S. Gómez, M.B. Ponce, F.J.B. Pedemonte, Effects of Laser Processing Parameters on Texturized Layer Development and Surface Features of Ti6Al4V Alloy Samples, Coatings 8 (2018), https://doi.org/10.3390/coatings8010006.

[62] J. Drelich, E. Chibowski, D.D. Meng, K. Terpilowski, Hydrophilic and Superhydrophilic Surfaces and Materials, Soft Matter 7 (2011) 9804–9828.

[63] S.Y. Liu, H.Q. Li, C.X. Qin, R. Zong, X.Y. Fang, The Effect of Energy Density on Texture and Mechanical Anisotropy in Selective Laser Melted Inconel 718, Mater. Des. (2020, 191,), https://doi.org/10.1016/j.matdes.2020.108642.

[64] T. Bhardwaj, M. Shukla, Effect of Laser Scanning Strategies on Texture, Physical and Mechanical Properties of Laser Sintered Maraging Steel, Mater. Sci. Eng. A 734 (2018) 102–109, https://doi.org/10.1016/j.msea.2018.07.089.

[65] Q. Bénard, M. Fois, M. Grisel, Roughness and Fibre Reinforcement Effect onto Wettability of Composite Surfaces, Appl Surf Sci 253 (2007) 4753–4758, https://doi.org/10.1016/j.apsusc.2006.10.049.

[66] A. Riveiro, T. Abalde, P. Pou, R. Soto, J. del Val, R. Comesaña, A. Badaoui, M. Boutinguiza, J. Pou, Influence of Laser Texturing on the Wettability of PTFE, Appl Surf Sci 515 (2020), https://doi.org/10.1016/j.apsusc.2020.145984.

[67] H. Qiang Dou, H. Liu, S. Xu, Y. Chen, X. Miao, H. Lü, X. Jiang, Influence of Laser Fluences and Scan Speeds on the Morphologies and Wetting Properties of Titanium Alloy, Optik (Stuttg) 224 (2020), https://doi.org/10.1016/j.ijleo.2020.165443.

[68] M. Lampin, R. Warocquier-Clérout, C. Legris, M. Degrange, M.F. Sigot-Luizard, Correlation between Substratum Roughness and Wettability, Cell Adhesion, and Cell Migration, J. Biomed. Mater. Res. 36 (1997) 99–108, https://doi.org/10.1002/(SICI)1097-4636(199707)36:1<99::AID-JBM12>3.0.CO;2-E.

[69] Z. Feng, H. Zhao, C. Tan, B. Zhu, F. Xia, Q. Wang, B. Chen, X. Song, Effect of Laser Texturing on the Surface Characteristics and Bonding Property of 30CrMnSiA Steel Adhesive Joints, J Manuf Process 47 (2019) 219–228, https://doi.org/10.1016/j.jmapro.2019.09.046.

[70] U. Maheshwera, R. Paturi, H. Devarasetti, S. Kumar, R. Narala, *Application Of Regression And Artificial Neural Network Analysis In Modelling Of Surface Roughness In Hard Turning Of AISI 52100 Steel*, 2018; Vol. 5.

[71] M. Mourabet, A. El Rhilassi, M.B. Ziatni, A. Taitai, Comparative Study of Artificial Neural Network and Response Surface Methodology for Modelling and Optimization the Adsorption Capacity of Fluoride onto Apatitic Tricalcium Phosphate. Universal J. Appl. Math. 2 (2014) 84–91, 10.13189/ujam.2014.020202.

[72] M. Khayet, C. Cojocaru, M. Essalhi, Artificial Neural Network Modeling and Response Surface Methodology of Desalination by Reverse Osmosis, J Memb Sci 368 (2011) 202–214, https://doi.org/10.1016/j.memsci.2010.11.030.

[73] S. Oh Comparison of a Response Surface Method and Artificial Neural Network in Predicting the Aerodynamic Performance of a Wind Turbine Airfoil and Its Optimization. *Appl. Sci. (Switzerland)* **2020**, *10*, 10.3390/APP10186277.